JCTC Journal of Chemical Theory and Computation

Article

Cite This: J. Chem. Theory Comput. 2018, 14, 2705−2720

pubs.acs.org/JCTC

AMOEBA Polarizable Force Field Parameters of the Heme Cofactor in Its Ferrous and Ferric Forms

Xiaojing Wu,[†] Carine Clavaguera,[*,†] Louis Lagardère,[‡,§] Jean-Philip Piquemal,[∥,⊥,#] and Aurélien de la Lande[*,†]

[†]Laboratoire de Chimie Physique, Université Paris Sud - CNRS, Université Paris Saclay, 15 Avenue Jean Perrin, 91405 Orsay Cedex, France

[‡]Sorbonne Université, CNRS, Institut Parisien de Chimie Physique et Théorique (IP2CT), 4 Place Jussieu, F-75005, Paris, France

[§]Sorbonne Université, Institut des Sciences du Calcul et des Données (ISCD), 4 place Jussieu, F-75005, Paris, France

[∥]Sorbonne Université, CNRS, Laboratoire de Chimie Théorique (LCT), 4 Place Jussieu, F-75005, Paris, France

[⊥]Department of Biomedical Engineering, The University of Texas at Austin, Austin, Texas 78712, United States

[#]Institut Universitaire de France, 75005, Paris, France

Supporting Information

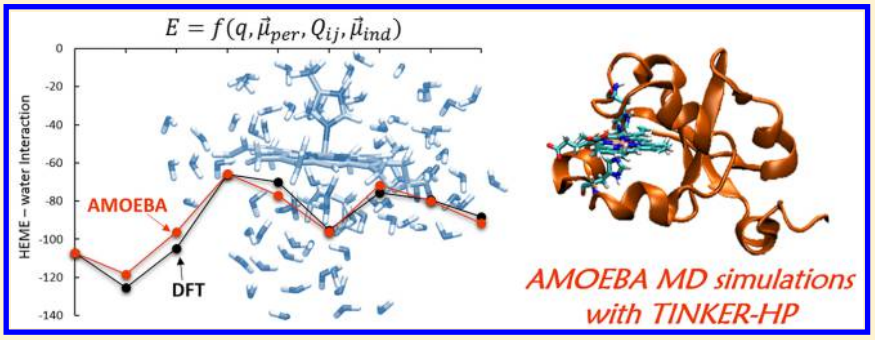

ABSTRACT: We report the first parameters of the heme redox cofactors for the polarizable AMOEBA force field in both the ferric and ferrous forms. We consider two types of complexes, one with two histidine side chains as axial ligands and one with a histidine and a methionine side chain as ligands. We have derived permanent multipoles from second-order Møller−Plesset perturbation theory (MP2). The sets of parameters have been validated in a first step by comparison of AMOEBA interaction energies of heme and a collection of biologically relevant molecules with MP2 and Density Functional Theory (DFT) calculations. In a second validation step, we consider interaction energies with large aggregates comprising around 80 H_2O molecules. These calculations are repeated for 30 structures extracted from semiempirical PM7 DM simulations. Very encouraging agreement is found between DFT and the AMOEBA force field, which results from an accurate treatment of electrostatic interactions. We finally report long (10 ns) MD simulations of cytochromes in two redox states with AMOEBA testing both the 2003 and 2014 AMOEBA water models. These simulations have been carried out with the TINKER-HP (High Performance) program. In conclusion, owing to their ubiquity in biology, we think the present work opens a wide array of applications of the polarizable AMOEBA force field on hemeproteins.

I. INTRODUCTION

Hemeproteins play important roles in diverse biological functions including transportation or storage of dioxygen (e.g., hemoglobin, myoglobin, neuroglobin), electron transport (e.g., cytochromes), or in enzymatic reactions (e.g., cytochromes P450). This remarkable diversity of functions results from the specific chemical structure of the heme motif, which consists of an iron cation chelated by the four nitrogen atoms of a deprotonated porphyrin ligand. The iron cation arranges in an almost planar geometry with one or two ligands completing the coordination sphere in axial position. The axial ligand may either be amino acid residues, typically histidine or methionine side chains, or exogenous ligands (O_2, NO, H_2O...). Both the ferrous and ferric forms of the iron cation can be stabilized by the complex. This ensemble of structural and redox properties confers distinct biological functions to hemeproteins. Intensive research in both experiments[1−4] and theoretical simulations[5−14] have been done to unravel the molecular mechanisms associated with the biological functions of hemeproteins.

Focusing on the modeling of the redox properties of hemeproteins, much progress has been realized over the past two decades.[7,8,10,15,16] Computational modeling is essential in this research field to help understand the variability of redox

Received: November 9, 2017
Published: April 9, 2018

DOI: 10.1021/acs.jctc.7b01128
J. Chem. Theory Comput. 2018, 14, 2705−2720

properties of different hemeproteins. For example, one can rationalize variations of redox potentials or of reorganization energies of hemeproteins from the secondary structure of the protein. Indeed, the presence of charged or polar chemical groups is important in determining the free energies of oxidation of hemes. It is now well documented that the redox properties of hemeproteins depend not only on the structure of the heme cofactor but also on the structure and on the dynamics of the protein matrix and on the hydration level of the proteins.[17] When interested in evaluating redox potentials or electron transfer rates, a particularly powerful approach consists of combining quantum mechanical (QM) methodologies to molecular dynamics (MD) simulations with molecular mechanics (MM) methodologies (i.e., classical force fields). We refer the reader to recent review papers detailing the different strategies employed so far in the literature to evaluate redox properties of proteins.[15,18,19] There are several parameters that impact the accuracy of computed redox properties: (i) the choice of the QM method to evaluate the intrinsic propensity of heme to lose an electron (ionization potential), (ii) the accuracy of the force field (FF) to describe the environment and its interaction with the heme, and (iii) the extensiveness of the conformational sampling of the proteins in the different redox states. Even though much progress has been realized in past decades in terms of the accuracy of redox property computations, numerical approaches are still far from reaching experimental precision. For instance, uncertainties of a few millivolts on the redox potentials which are reachable by electrochemical means correspond to an accuracy of less than 1 kcal/mol on free energies of oxidation. A key challenge is to accurately describe electrostatic interactions between the heme cofactor and its environment (protein, water, counterions...). Indeed the change from the +II to +III (or *vice versa*) induces significant conformational rearrangements of the environment. Previous studies showed that inclusion of electrostatic induction in classical FFs is mandatory to capture reorganization of surrounding atoms.[17,20−22] Indeed, the associated reorganization energy is related to the optical dielectric constant of the medium and can only be reproduced by polarizable FFs.[8,15,18] Another fundamental limitation of standard FFs is the monopolar representation of the permanent electron cloud of molecules.

Force field parameters for heme have been proposed for various nonpolarizable FFs.[23−30] In this work, we are interested in the Atomic Multipole Optimized Energetics for Biomolecular Applications (AMOEBA) force field implemented in the Tinker program package (version 7.1.2).[31] AMOEBA stands as a highly accurate FF for water[32,33] and for ion hydration[34−38] and to reproduce the structures and thermodynamics of organic molecules and biomolecules.[39−43] The AMOEBA water model was also compared to the Drude polarizable force field[44] to evaluate reorganization free energy for electron self-exchange in aqueous Ru(II)−Ru(III).[45] Electrostatic interactions between permanent charge distributions are accounted for by sets of permanent monopolar, dipolar, and quadrupolar moments centered on atoms. Moreover, AMOEBA implements an induction model which allows reproduction of the anisotropy and the nonadditivity of the molecular polarization response. Furthermore, recent developments have introduced short-range penetration corrections between molecules.[46−48] We are not aware of any MD simulation of hemeproteins carried out with AMOEBA, a situation undoubtedly related on one hand to the lack of parameters for the heme cofactor and on the other hand to the computational cost of such simulations with common computer codes. Indeed, as one can expect, such a sophisticated FF is far more expensive than standard force fields developed to study biomolecules. In that regard, noticeable algorithmic developments in the Tinker-HP (High-Performance) software[49] have been carried out by some of us which enable long (>100 ns) MD simulations on biological systems with AMOEBA.[50,51] The development of AMOEBA FF parameters of heme is therefore timely. We report here to the best of our knowledge the first sets of AMOEBA parameters for the heme cofactor in both the ferric and ferrous states.

The details of the parametrization procedure will be given in section II. The sets of parameters will be validated against quantum chemistry calculations in section III. The results show a clear improvement of interaction energies between heme and surrounding molecules compared to point-charge FF. Finally, we will report in section IV, to the best of our knowledge, the first nanosecond MD simulations of a cytochrome with AMOEBA as implemented in TINKER-HP.[49]

II. METHODOLOGY

II.A. The Amoeba Potential Energy Model. The functional form of the potential energy computed by AMOEBA is given by eq 1:

$$U = U_{\text{bond}} + U_{\text{angle}} + U_{\text{cross}} + U_{\text{opp}} + U_{\text{torsion}} + U_{\text{vdW}} + U_{\text{ele}}^{\text{perm}} + U_{\text{ele}}^{\text{ind}} \quad (1)$$

The first five terms are the valence interactions including bonds, angles, bond-angle cross coupling terms, out-of-plane deformations, and torsional rotations. AMOEBA uses mathematically flexible expressions that go beyond the harmonic approximation for the intramolecular terms. These terms have the same functional forms as those used by the MM3 force field.[52] Analytical expressions for each of these terms can be found in ref 39. The last three terms of eq 1 gather intermolecular interactions. U_{vdw} refers to van der Waals interactions and is calculated with Halgren's buffered 14−7 function. This function yields a repulsive region softer than the Lennard-Jones 6−12 function but steeper than typical Buckingham exp-6 formulations. $U_{\text{ele}}^{\text{perm}}$ collects the electrostatic interactions between permanent multipoles. Monopoles, dipole vectors, and quadrupole tensors are positioned on each atom site in order to reproduce the molecular electrostatic potentials accurately. These permanent atomic multipoles are defined with respect to local frame and maintain a constant orientation during simulations. Finally, $U_{\text{ele}}^{\text{ind}}$ refers to interactions between permanent charges and induced dipoles. Atomic polarizabilities are included to determine induced dipole moments on each polarizable site. Electronic induction is achieved via an interactive atomic dipole induction scheme.[51] The induced dipole at site *i* further polarizes all other sites until the induced dipoles at each site reach convergence. The simulations use a preconditioned conjugate gradient solver coupled to Kolafa's Always Stable Predictor-Corrector (ASPC) algorithm.[53] To avoid the polarization catastrophe phenomenon, AMOEBA employs Thole's short-range damping method.[54] In the present work, we do not include short-range penetration corrections.[46,48]

II.B. Parametrization Strategy. We have followed the standardized parametrization protocol of AMOEBA FF.[55] As recalled in the Introduction, the coordination sphere of Fe in heme can encompass various chemical groups depending on

DOI: 10.1021/acs.jctc.7b01128
J. Chem. Theory Comput. 2018, 14, 2705−2720

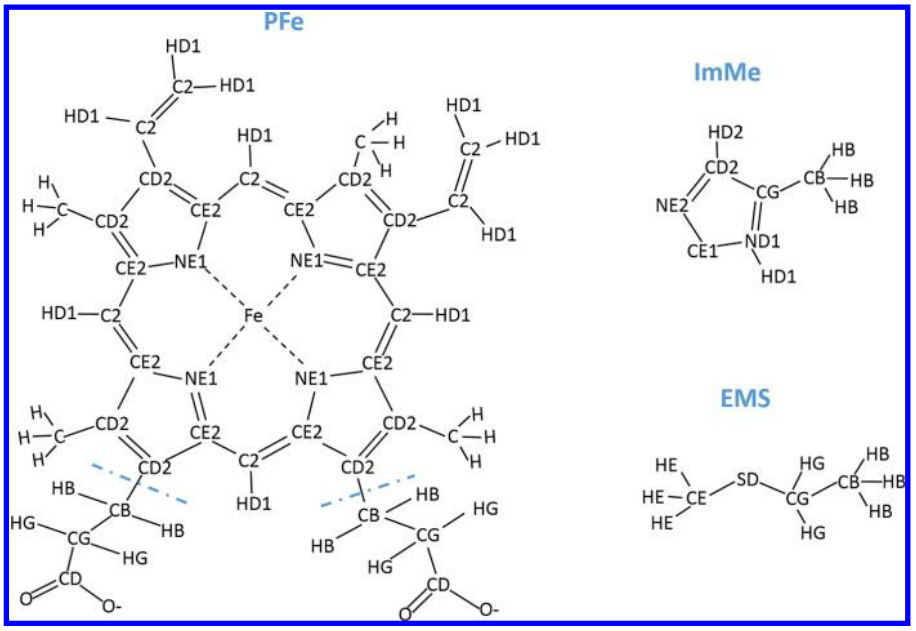

Figure 1. Heme structure, ligand models, and atom definitions for the parametrization procedure.

the protein of interest. For example, the Fe cation can be coordinated by one or two histidine residues (*e.g.*, cytochrome P450 or cytochrome b_5), by one histidine and one methionine residue (cytochrome c551), or by histidine and small ligands (like O_2, NO...). These different coordination spheres would necessitate distinct sets of parameters. In this work, we are primarily interested in six-coordinated hemes with either two histidines or one histidine and one methionine axial ligand. Such coordination patterns are, for instance, frequently encountered in cytochromes or globins. In our first parametrization attempts, we considered the full six-coordinated complexes; however, we experienced difficulties in obtaining reliable multipoles, and we therefore decided to adopt another strategy. Our approach consists of parametrizing the four-coordinated iron porphyrin ($PFe^{II/III}$), on one hand, and the axial ligands separately. This approach is justified when the axial ligands are either histidine or methionine residues by the fact that charge transfer from the iron cation toward the ligand is rather small. Indeed, charge transfer from the axial ligands to the iron-porphyrin complex amounts to 0.05 e^- and 0.15 e^- in the ferrous and ferric states respectively, based on Density Functional Theory (DFT) calculations combined with the iterative Hirshfeld[56] electronic population scheme (Table S1). We expect the multipolar description of the FF to describe sufficiently well the interaction between PFe and the axial ligands. The chemical structure of the PFe group used during the parametrization protocol is depicted in Figure 1. This PFe group has been further truncated into three fragments as shown in the figure. The amino acid backbone atoms of histidine and methionine have been modeled as methyl-imidazole (ImMe) and ethyl-methyl-sulfide (EMS), respectively. Note that this strategy also assumes that no spin density is transferred from the iron porphyrin core to the axial ligands (see Table S1).

Figure 1 depicts the atom types for all atoms. For the intramolecular terms, the atom types and classes of PFe atoms and the two ligands have been defined by analogy with parameters from the AMOEBA-2013 FF for proteins.[43] For example, the AMOEBA classes and types of atoms CD2, CE2, and NE1 within the porphyrin ligand were transposed from the analogous atoms of the five-membered ring of the tryptophan residue. NE1 is nitrogen atoms pertaining to the azole ring, CE2 is sp^2's of the azole cycle linked to NE1 and to one sp^3 carbon and one sp^2 carbon. Finally, CD2 is sp^2's of the azole cycle linked to two other sp^2 carbon atoms. The valence parameters (bond stretching, angle bending, torsions, van der Waals, and polarizabilities) were taken from the set without modification. The van der Waals and atomic polarizability for Fe were taken from the work of Semrouni et al. for the ferrous state.[34] The same van der Waals parameters are here for both the ferrous and ferric state. This has been common practice for simulations of hemeproteins using more standard force fields.[18,27] We actually think that for iron cations nested at the heart of the porphyrin ligand in well-defined coordination spheres, the differences of nonbonding interactions between the two redox states can be captured by adequately tuned sets of multipoles on the metal ion and its coordination sphere. This methodological strategy will be validated extensively in sections II and III.

A central aspect of the parametrization procedure is the fitting of multipoles for PFe. The sets of multipoles have to be different in the ferrous and ferric redox states. To that end, we have optimized the geometry of the [PFe-ImMe-EMS] complex by DFT calculations with the OPTX-PBE functional[57,58] and the DZVP-GGA basis set.[59] These calculations have been carried out with deMon2k.[60] To avoid spurious electronic delocalization between the iron cation and the carboxylate functions, the latter have been protonated during geometry optimizations. The OPTX-PBE functional has been chosen for its good performance to reproduce the electronic energies of different spin states in transition metal complexes.[61,62] deMon2k relies on auxiliary fitted densities to calculate the Coulomb and exchange correlation energies and potentials.[63] The auxiliary basis sets are automatically generated by the program.[59] We chose the GEN-A2 for H and C, and the more flexible, therefore more accurate, GEN-A2* for Fe, N, and S. Geometry optimizations have been conducted in the singlet, triplet, and quintet spin states for the ferrous state and in the doublet, quartet, and sextet spin states for the ferric state. We

DOI: 10.1021/acs.jctc.7b01128
J. Chem. Theory Comput. 2018, 14, 2705−2720

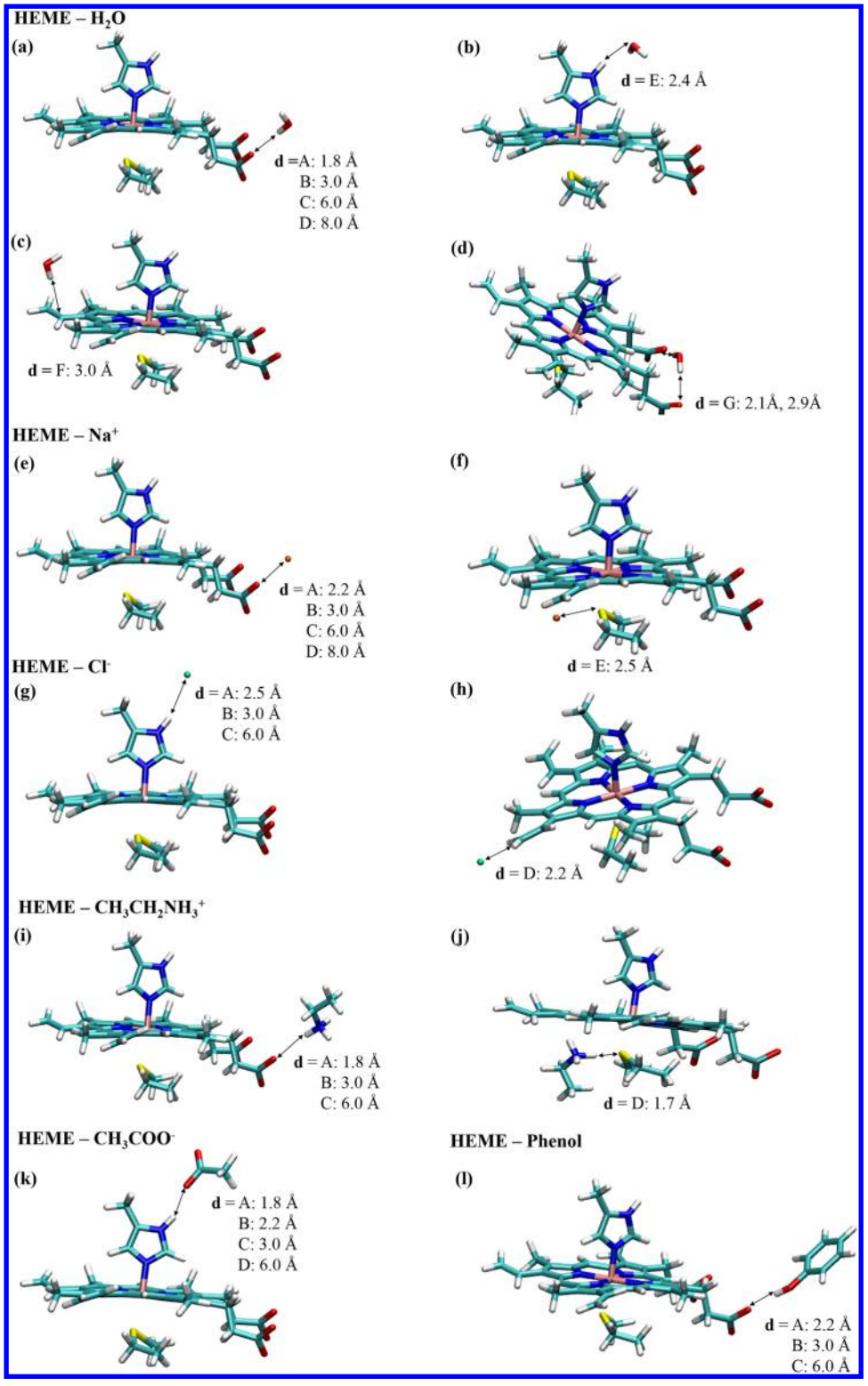

Figure 2. Geometries of heme interacting with molecules used in the validation of the AMOEBA FF parameters. Picture made with VMD.[78]

have found the singlet and doublet spin states to be the most stable for ferrous and ferric redox states, respectively, by 0.72 and 0.57 eV. We have restricted our parametrization procedure to these two spin states.

After geometry optimization, the structures have been fragmented according to the partition of Figure 1. Hydrogen atoms have been added at the cutting positions between the porphyrin ring and the propionate groups, and we have reoptimized the hydrogen atom positions. Following the AMOEBA parametrization procedure, single point calculations of each fragment have been performed at the MP2/cc-pVDZ level of theory with Gaussian 09.[64] The ground states of four-coordinated iron-porphyrins are of intermediate spin. MP2 calculations on the fragments have been carried out in the lowest spin state to be consistent with the lowest spin state of the six-coordinated iron-porphyrin. The Distributed Multipole

DOI: 10.1021/acs.jctc.7b01128
J. Chem. Theory Comput. 2018, 14, 2705−2720

Analysis (DMA) has been carried out from the MP2 electron density using the GDMA program (version 2.2.11) and the original DMA algorithm.[65−68] The default relative atomic radii used in the DMA algorithm have been chosen except for hydrogen, for which a value of 0.31 has been chosen. This value was previously shown to be appropriate to avoid erroneous charges during the DMA procedure.[69]

The POLEDIT program available in Tinker[31] has been subsequently run on the GDMA outputs with the suggested polarizability values. All atoms are placed into a single polarization group by default. This resulting version of multipoles is obtained directly from the DMA procedure. This set of parameters will be referred to as "AMOEBA DMA." Another approach to derive atomic multipoles involves an optimization against the QM electrostatic potential around the system. The AMOEBA DMA multipole values have been used as starting values to the fitting against the MP2/cc-pVDZ electrostatic potential. The DMA partial charges are held fixed during the potential fitting process, while dipoles and quadrupoles are readjusted. The final gradient convergence value has been set to 0.5 kcal mol^{-1} $electron^{-2}$ to avoid overfitting. Indeed, a tighter convergence criterion can lead to multipoles that depend strongly on the geometry used for the extraction, and therefore that are less transferable. We will refer to this second set of parameters as "AMOEBA FIT." Finally, according to the defined atom types, the multipole values have been averaged over the equivalent atoms. The procedure was carried out for each fragment. Two versions of each multipole set have been created for both ferrous and ferric states. At the end, all the fragments have been combined by removing excess hydrogens, and the global charge has been adjusted to be −2 and −1 for ferrous and ferric states, respectively. In summary, four parameter sets have been generated and named Fe^{II} AMOEBA DMA, Fe^{II} AMOEBA FIT, Fe^{III} AMOEBA DMA, and Fe^{III} AMOEBA FIT. They will be now tested against quantum mechanical calculations. The parameters are available in the SI.

III. VALIDATION AND SIMULATIONS

In section III, we validate the different AMOEBA parameter sets on the calculation of interaction energies between the heme and its environment. We start by gas phase interaction energies (IE) between the [PFe-ImMe-EMS] complex and different molecules relevant to biological systems. We continue by calculating IE with large clusters of water molecules. We also address the transferability of our parameters for the [PFe-$(ImMe)_2$] complex. We finally conclude the section by the adjustment of the internal bond and valence angle terms to tune the geometry of the iron first coordination shell.

III.A. Computational Details. As a first test of the sets of AMOEBA parameters, we here report interaction energies between the [PFe-ImMe-EMS] and various molecules in the gas phase. The IE between the iron complex and a molecule (M) is defined as

$$\Delta E_{int} = E([PFe, M]) - E([PFe]) - E(M) \quad (2)$$

where $E([PFe,M])$ is the energy of the supramolecular complex and $E([PFe])$ and $E(M)$ are the energies of the two fragments. For each supramolecular system, the geometry has been constructed by associating the [PFe^{II}−ImMe−EMS] complex, geometrically optimized in the absence of the partner M, with the geometry of the fragment. A restrained geometry optimization of the supramolecular ensemble has been carried out at the DFT level, freezing the geometry of the heme partner, and optimizing only the internal geometry of partner M. In these restrained optimizations, we have eventually further imposed the distances between the two partners to a given value. Basis set superposition error corrections have not been computed. The list of molecules includes H_2O, $CH_3CH_2NH_3^+$ (a model of lysine side chain), CH_3COO^- (a model of aspartate and glutamate side chains), phenol (a model of tyrosine side chain), and the chlorine and sodium ions. This is a list of representative types of interactions one can find in hemeproteins between the heme cofactors and its environment. In particular, charged or polar residues are known to play a special role in determining redox properties. For example, in flavohemoglobin, a lysine residue is hydrogen bonded to one propionate group of the heme,[70,71] and a glutamate residue interacts with axial histidine residues.[70] Tyrosine residues have also been found to interact with heme propionates, for instance, in cytochrome *c* oxidase.[72] It is therefore important to assess whether the parameters developed in this work are able to accurately reproduce the associated interaction energies. The various supramolecular complexes are depicted in Figure 2.

Two types of QM calculations have been carried out, relying either on DFT (B3LYP[73]) or on MP2. Note that we have tested B3LYP-D3 calculations for some complexes and found negligible effects of dispersion on the computed interaction energies. We mention that convergence of Hartree−Fock or the DFT self-consistent field of deprotonated heme is tedious in the gas phase, especially for the ferric state. Indeed, the terminal propionate groups tend to be oxidized instead of the iron cation, eventually causing severe self-consistent field (SCF) convergence issues and unexpected electronic structures. It was therefore not always possible to obtain QM results for some geometries. MP2 single-point calculations have been performed within the Resolution of the Identity (RI) approach using the TZVP basis set for all atoms with the Turbomole 7.1 program.[74] DFT single-point energies have been calculated with deMon2k at the B3LYP/TZVP level (DZVP-GGA for Fe) and with the auxiliary function set GEN-A2* for all atoms. An adaptive grid of accuracy 10^{-8} Ha was defined to integrate the exchange correlation energy and potential.[75] Exact exchange was computed via a variational fitting of the Fock potential.[76]

For the FF calculations, the interaction energies with AMOEBA have been computed with the ANALYZE program from the TINKER package. The parameters of the small molecules and ions are taken from the AMOEBA-2013 parameter set for proteins. For H_2O, two versions of the AMOEBA water model, water03[32] and water14,[33] are tested. For $CH_3CH_2NH_3^+$ and CH_3COO^-, sets of multipoles have been determined with the previously described procedure for the heme. The energies entering eq 2 were calculated with eq 1 (AMOEBA). The AMOEBA interaction energies therefore include energy differences from the van der Waals, permanent electrostatic, and induction contributions to the energy. We have also tested a nonpolarizable FF based on the permanent point charge model. For this FF, the reported interaction energies include van der Waals contributions calculated with a 12−6 Lennard-Jones potential and a charge−charge Coulomb interaction. The parameters of vdW are taken from the CHARMM for ferrous heme.[27] The punctual charges have been derived by an iterative Hirshfeld (IH) population analysis[56] as implemented in deMon2k.[77] For water, the IH charges are close to those given by the TIP3P water model. All the computed interaction energies can be found in Table S2.

DOI: 10.1021/acs.jctc.7b01128
J. Chem. Theory Comput. 2018, 14, 2705−2720

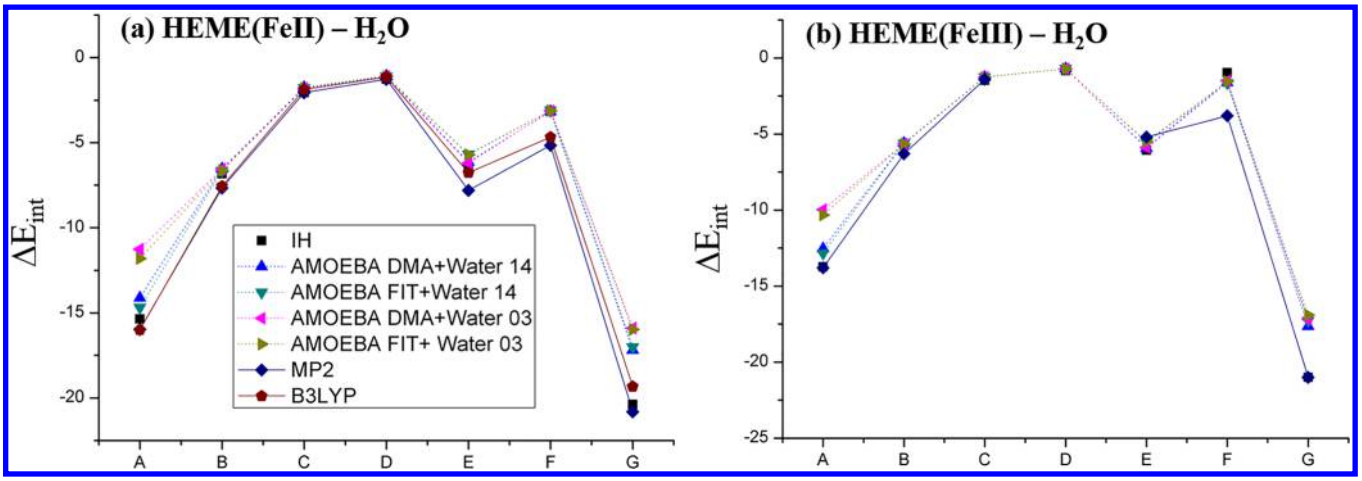

Figure 3. Heme–water interaction energies (kcal/mol) of the different geometries represented in Figure 2. Left, results of ferrous state; right, results of ferric state.

Table 1. Interaction Energy Differences in kcal/mol Obtained at the Various Computational Levels with Respect to the MP2/TZVP Reference

geometry	B3LYP	IH	AMOEBA DMA + water14	AMOEB FIT + water14	AMOEBA DMA + water03	AMOEBA FIT + water03
			HEME(FeII) − H_2O			
A	0.03	0.61	1.86	1.28	4.72	4.18
B	0.11	0.85	1.13	1.02	1.10	1.03
C	0.19	0.00	0.30	0.28	0.26	0.25
D	0.14	0.01	0.20	0.19	0.17	0.16
E	1.03	1.14	1.67	2.13	1.61	2.10
F	0.49	2.02	1.99	2.04	2.03	2.04
G	1.48	0.42	3.62	3.80	4.92	4.83
			HEME(FeIII) − H_2O			
A	n.c.[b]	0.07	1.28	0.95	3.83	3.48
B	n.c.	0.60	0.70	0.69	0.65	0.64
C	n.c.	0.06	0.14	0.15	0.13	0.14
D[a]	n.c.	0.00	0.12	0.12	0.11	0.11
E	n.c.	0.86	0.74	0.34	0.69	0.30
F	n.c.	2.85	2.19	2.16	2.30	2.26
G	n.c.	0.00	3.36	3.73	3.81	4.10

[a]Neither MP2 nor B3LYP calculations converged for geometry D in the ferric state. For this series, IH is taken arbitrarily as a reference. [b]The B3LYP SCF could not converge.

III.B. Interaction between Heme and Single Molecules. *Heme–Water.* We start our discussion with results on IE between heme and a water molecule (see Figure 2a–d). Geometries a correspond to a water molecule engaged in hydrogen bonding with one propionate side chain with different lengths (1.8 Å for A, 3.0 Å for B, 6.0 Å for C, 8.0 Å for D). Geometry b,E corresponds to a hydrogen-bond interaction from the NH group of ImMe toward the oxygen atom of water. The equilibrium distance resulting from geometry optimization with DFT amounts to 2.4 Å. Geometry c,F corresponds to a weak OH–π interaction between one C=C double bond of heme and one hydrogen atom of water, with an interaction distance of 3.0 Å. Finally, geometry d,G involves a double hydrogen-bond interaction with the water bridging the two propionate side chains with the O–H distances amounting to 2.1 and 2.9 Å. Results are plotted in Figure 3. For geometries A to D, all the methods give the same trend. As expected, the interaction becomes less favorable as the distance increases.

The interaction energy differences for each method with respect to MP2 are provided in Table 1. For geometries C and D, in which the hydrogen bond is weak (>3 Å), all the methods give an IE within 0.3 kcal/mol to that given by MP2. For such long-distance interactions, a monopolar description of the electron density is likely to be valid and therefore accounts for the convergence of nonpolarizable and AMOEBA FF results. For geometries A and B, the differences are more significant between the methods. Among them, the IH results are the closest to MP2 with an error of less than 1.0 kcal/mol. For AMOEBA calculations on geometry B, all parameter sets give similar results. For geometry A, a larger error is found with the water03 model. A plausible explanation for this discrepancy may be the lack of correction for penetration effects.[46] These effects are not taken into account by the version of the AMOEBA FF used in this work. On the other hand, the water14 model is able to significantly reduce the error with respect to MP2 due to the reparameterization of the electrostatic term.

For geometry E, the results for IH and AMOEBA are almost similar. The differences of IE with respect to MP2 are ca. 2 kcal/mol for the ferrous state, while they are only ca. 0.7 kcal/mol for the ferric state. The results with the different FFS for geometry F are similar for the ferrous state with a difference at

DOI: 10.1021/acs.jctc.7b01128
J. Chem. Theory Comput. 2018, 14, 2705–2720

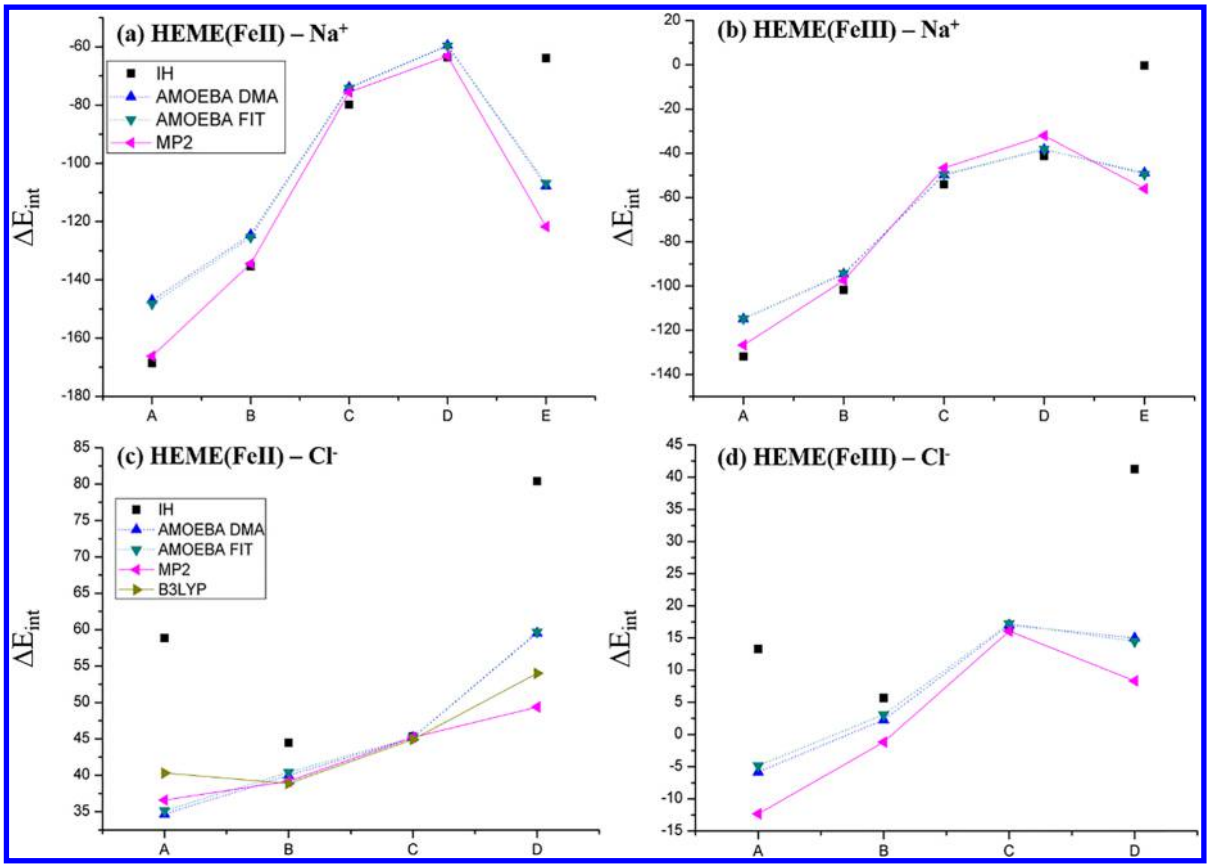

Figure 4. Heme−ions (Na^+ and Cl^-) interaction energies (kcal/mol) of the different geometries represented in Figure 2. Left: results for the ferrous state. Right: results for the ferric state. B3LYP calculations for the ferric states are not reported because of self-consistent-field convergence issues.

ca. 1.6 kcal/mol. However, regarding the ferric state, AMOEBA gives a difference of 2.1 kcal/mol, while IH has a difference of 2.9 kcal/mol. For geometry G, the error for both states is ca. 3.5 and 5 kcal/mol for the water14 and water03 parameters, respectively. As for geometry A, we find that the water14 model seems to perform better, and the nonpolarizable model gives as accurate results.

Heme−Atomic Ions. Five geometries were created to test the accuracy of the interaction with the sodium cation. As shown in Figure 2e, we have investigated interactions with either the propionates groups (A, B, C, or D) or the sulfur atom of the EMS ligand (E). The results obtained with the different computational methods are plotted in Figure 4 for the ferrous and ferric states (panels a and b, respectively). For the A, B, C, and D series, the interaction becomes less favorable with increasing the distance, while the difference between the various methods decreases. This is similar to what was found for the interaction with H_2O. For geometries C and D in the ferrous state, all methods are within 4 kcal/mol of the MP2 values. The energy differences are larger (ca.7 kcal/mol) for the ferric state. For geometries A and B, IH gives good results with errors lower than 5 kcal/mol. With the AMOEBA FF, we obtain differences around 19 and 9 kcal/mol for geometries A and B, respectively. For geometry E, AMOEBA gives a difference of 14 and 7 kcal/mol with respect to MP2 for the ferrous and ferric states, respectively. For this type of interaction involving a large and polarizable group (thioether), AMOEBA represents a clear improvement over nonpolarizable FF for which differences larger than 55 kcal/mol are found.

We now turn to interaction with chlorine (Figure 2). Geometries A, B, and C correspond to interaction with the ImMe, while geometry D corresponds to a weak dispersive interaction between Cl^- and one C=C bond or the porphyrin ring. Results are shown in Figure 4 (panels c and d). We remark that as a consequence of the overall −2 or −1 charge of the heme complex in the ferrous and ferric states, the interaction energies with the chlorine anion are almost always positive. Nevertheless, in actual biosystems, other interactions with positively charged residues may counterbalance the repulsive interaction with heme so that anions may still approach them. It is therefore important to test the capability of the AMOEBA parameters to correctly describe the electrostatic interactions between heme and anions. For geometries A, B, and C, AMOEBA reproduces the increase of IE with the distance between heme and Cl^-. The difference between AMOEBA and MP2 amounts to 2 kcal/mol in the ferrous states and is a little bit larger in the ferric state. The IH curves exhibit, on the other hand, opposite trends, failing to reproduce even qualitatively the evolution of IE provided by QM methods. We could trace back this discrepancy in the unbalanced treatment of electrostatic and Lennard-Jones interactions. AMOEBA provides a better description of the noncovalent interaction between atomic anions and heme. For geometry D also, AMOEBA gives better results for the ferrous state than IH by ca. 21 kcal/mol. This large difference can be mainly due to the interaction with the C=C bond. Here again, we see the advantage of using a polarizable force field.

Heme−$CH_3CH_2NH_3^+$. As shown in Figure 2, geometries (i) A, B, C, and D represent hydrogen-bonded interactions

DOI: 10.1021/acs.jctc.7b01128
J. Chem. Theory Comput. 2018, 14, 2705−2720

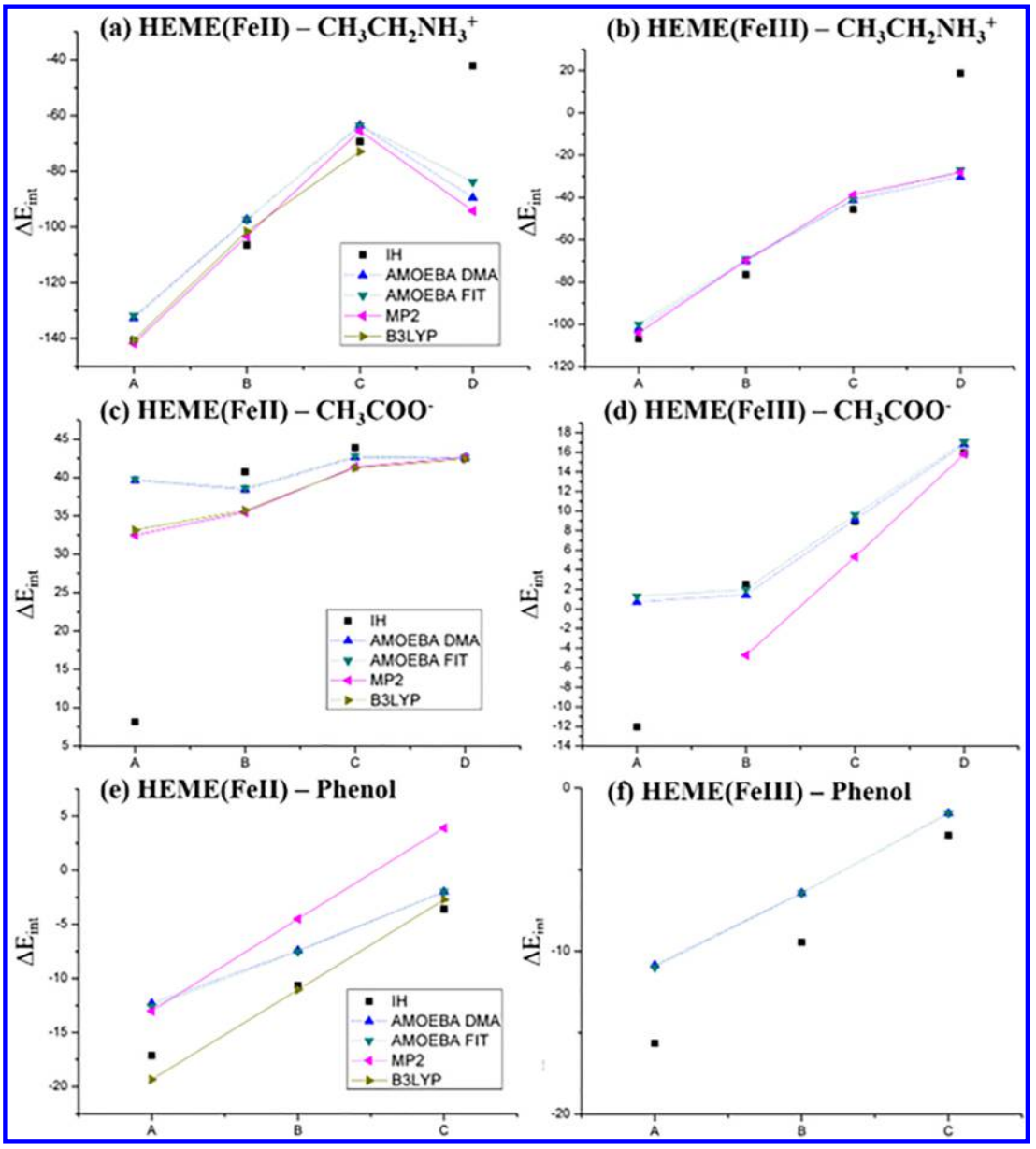

Figure 5. Heme−molecule interaction energies (kcal/mol) of the different geometries represented in Figure 2. Left: results for the ferrous state. Right: results for the ferric state. Missing points for quantum mechanical methods (MP2 and/or B3LYP) are due to self-consistent-field convergence issues.

between the propionate side chain of heme and $CH_3CH_2NH_3^+$ with increasing length. Geometry D involves an interaction with the thioether. The values of the interaction energies are plotted in Figure 5a for the ferrous state and 5b for the ferric state. Overall, we find that AMOEBA gives a satisfactory treatment of the interaction between this cationic organic species and the heme. IH also gives good results for geometries A, B, and C; however, it fails for geometry D with a difference ca. 50 kcal/mol with MP2. This finding is reminiscent of the difficulty of treating the interaction between Na^+ and the thioether ligand, illustrating again the advantage of FF relying on a balanced treatment of electrostatic interactions involving permanent multipoles and induced dipoles. That said, like for geometry D, it is probably not likely to be encountered often in the course of MD simulations owing to the short distance between the two interacting partners.

Heme−CH_3COO^-. Geometries A, B, C, and D involve a hydrogen bond between ImMe and CH_3COO^- with increasing length (Figure 2k). The values of the interaction energies are plotted in Figure 5. At long distances, all the FF results are very close to the QM based method (<0.1 kcal/mol), for both redox states. When decreasing the hydrogen bond length, the interaction between the two anionic partners becomes less unfavorable. AMOEBA as well as IH adequately reproduce the trend provided by MP2 or B3LYP. One noticeable exception is geometry A, which is overstabilized with a simple point-charge model (IH).

Heme-Phenol. As shown in Figure 2l, geometries A, B, and C represent the hydrogen-bond interaction between the phenol and the propionate side chain of heme. Interaction energies are given in Figure 5. We first remark on a systematic difference of 6.5 kcal/mol between MP2 and B3LYP for the ferrous state, which is difficult to interpret. The IH results are close to the

DOI: 10.1021/acs.jctc.7b01128
J. Chem. Theory Comput. 2018, 14, 2705−2720

B3LYP ones, while the AMOEBA results lie in between the B3LYP and MP2. For the ferric state, we could not converge either MP2 or DFT calculations of the heme cofactor. A similar trend than the ferrous state is obtained with the three FFs.

Summary. In summary, AMOEBA is globally in good agreement with QM methods (MP2 and DFT). This is especially true for interaction with highly polarizable groups such as S, C=C double bonds, or anions like Cl^-. Finally, no large difference has been observed between the two sets of multipoles (DMA or FIT). We can observe that the FIT version gives slightly better results than the DMA one by ca. 1 kcal/mol. For short distances, larger deviations between AMOEBA and QM have been found.

III.C. Heme within Droplets of Water. In the previous section, we validated our AMOEBA parameters looking at interaction energies between the [$PFe^{II/III}$−ImMe−EMS] complex and various molecules. We now address collective effects by computing interaction energies between the [$PFe^{II/III}$−ImMe−EMS−$(H_2O)_6$] complexes and a large ensemble of water molecules. Note that we have included six water molecules around the propionate moieties of the heme to avoid spurious oxidation by the Fe^{III} cation. We also address in this section the transferability of the parameters to the description of the [PFe^{II}−$(ImMe)_2$−$(H_2O)_6$] complex.

In a preliminary step, MD simulations have been carried out with the PM7 semiempirical method and the CUBY4 environment.[79] Details of the PM7MD simulations can be found in the SI. The heme complexes ([PFe^{II}−ImMe−EMS] and [PFe^{II}−$(ImMe)_2$]) are embedded in droplets of water comprising around 1850 water molecules. After geometry optimization, MD simulations have been carried out for 80 ps. Interaction energies have been computed according to eq 2 with energies calculated using deMon2k (DFT) or Tinker (AMOEBA). The normalized autocorrelation functions of the IE obtained with AMOEBA approach zero in periods of a few hundreds of femtoseconds to a few picoseconds (Figure S1). Consequently, we have extracted snapshots for subsequent interaction energy calculations every 2 ps during the last 60 ps, leading to a total of 30 geometries for each complex that can be considered as uncorrelated. To make the DFT level tractable, the geometries have been pruned to retain only the water molecules within less than 8 Å from the iron cation. The pruned geometries typically comprise 75 to 80 H_2O (for a total of 330 atoms on average). To carry out these computationally very intensive calculations, the Coulomb, local exchange-correlation, and nonlocal exact exchange contribution to the Kohan−Sham potential have been computed with auxiliary fitted quantities.[63,76] We have used the DZVP-GGA/GEN-A2* combination of atomic orbital and auxiliary basis sets. The grid accuracy to integrate the exchange correlation energy and potential has been set to 10^{-8} Ha. Calculations have been carried out with B3LYP,[73] PBE,[58] and PBE0.[80] For complexes in the ferrous states, SCF convergence has been reached with a tolerance of 10^{-7} Ha on the SCF energy and 10^{-6} on density fitting coefficients. For the ferric state, SCF convergence is much more difficult to obtain on all the complexes, and tolerance thresholds have been set to 10^{-4} Ha and 4.10^{-4} for some of them. However, we have verified on nine geometries for which tight convergence could be reached up to 10^{-7} Ha and 10^{-6} respectively, that the computed interaction energies are within 0.05 kcal/mol of those obtained with the looser 10^{-4} Ha and 4.10^{-4} convergence thresholds (Table S3).

Results are summarized in Table 2 for PBE0 and in Table S4 for PBE and B3LYP. The full list of IE is given in Table S5. For each complex, we report the average difference between the DFT and force field interaction energies ($\langle\Delta IE\rangle$) over the series and the associated standard deviation ($\sigma_{(\Delta IE)}$). We also report the Root-Mean-Square Error (RMSE) and the linear correlation coefficient between DFT results and FF results (R^2). We start by remarking noticeable differences among DFT methods for the [PFeII−ImMe−EMS−$(H_2O)_6$] complex. On one hand, PBE and PBE0 give similar IEs, with an average difference of *ca.* 3 kcal/mol. On the other hand, interaction energies calculated with B3LYP are shifted by 30 kcal/mol with respect to both PBE and PBE0 (Table S4). This discrepancy among various DFT XC functionals is large and illustrates the difficulty of obtaining reference values for validating our FF parameters. Recent benchmark calculations of relative energies of large water clusters against CCSD(T)/CBS (Complete Basis Set Limit) showed the sensitivity of such computations with XC functionals.[81] The authors recommended the use of range-separated hybrids (ωB97XD[82] or LC-ωPBE-D3[83,84]) or meta-GGA global hybrids (M05-2X[85]) for this type of calculation. These classes of DFT functionals are not currently available in the version of deMon2k we are using. PBE0 was ranked before PBE and B3LYP in this study, and we will mainly base our discussion on the PBE0 results.

Table 2. Average Interaction Energy (kcal/mol), Standard Deviation, RMSE, and Linear Correlation Coefficient between DFT (PBE0) Results and Force Field Results

		AMOEBA			
		DMA	FIT	DMA	FIT
	IH	water14	water14	water03	water 03
		[PFe^{II}ImMe−EMS−$(H_2O)_6$]			
$\langle\Delta IE\rangle$	−26.36	0.95	2.27	1.91	3.29
$\sigma_{(\Delta IE)}$	14.72	8.35	8.06	11.82	11.55
RMSE	30.07	8.26	8.25	11.77	11.83
R^2	0.70	0.86	0.87	0.73	0.74
		[PFe^{III}ImMe−EMS−$(H_2O)_6$]			
$\langle\Delta IE\rangle$	−25.84	−3.74	−2.46	−4.37	−2.93
$\sigma_{(\Delta IE)}$	13.26	7.82	7.57	10.02	10.06
RMSE	28.91	8.52	7.80	10.73	10.26
R^2	0.71	0.87	0.88	0.78	0.78
		[PFe^{II}−$(ImMe)_2$−$(H_2O)_6$]			
$\langle\Delta IE\rangle$	39.27	13.04	14.84	14.02	15.91
$\sigma_{(\Delta IE)}$	17.68	7.18	7.22	8.41	8.57
RMSE	42.94	14.82	16.44	16.27	18.00
R^2	0.62	0.94	0.94	0.93	0.93

We start our discussion with the [$PFe^{II/III}$−ImMe−EMS−$(H_2O)_6$] complex. The interaction energies computed with the nonpolarizable FF (using IH charges) lead to an average shift larger than 23 kcal/mol with respect to the PBE0 results. The scattering of the computed data is also large. As can be seen in Figure 6 (top, black points) the agreement with DFT is poor. This is reflected by a correlation coefficient of only 0.7. IEs obtained with AMOEBA are much more satisfactory, as seen from the figure and from the values of R^2. The agreement between AMOEBA and DFT (either PBE or PBE0) is especially good when we use the 2014 AMOEBA water model with R^2 approaching 0.9. The RMSE drops from 30 to 8.2 kcal/mol between the nonpolarizable FF and AMOEBA. These are very satisfactory results, indicating that moving from

DOI: 10.1021/acs.jctc.7b01128
J. Chem. Theory Comput. 2018, 14, 2705−2720

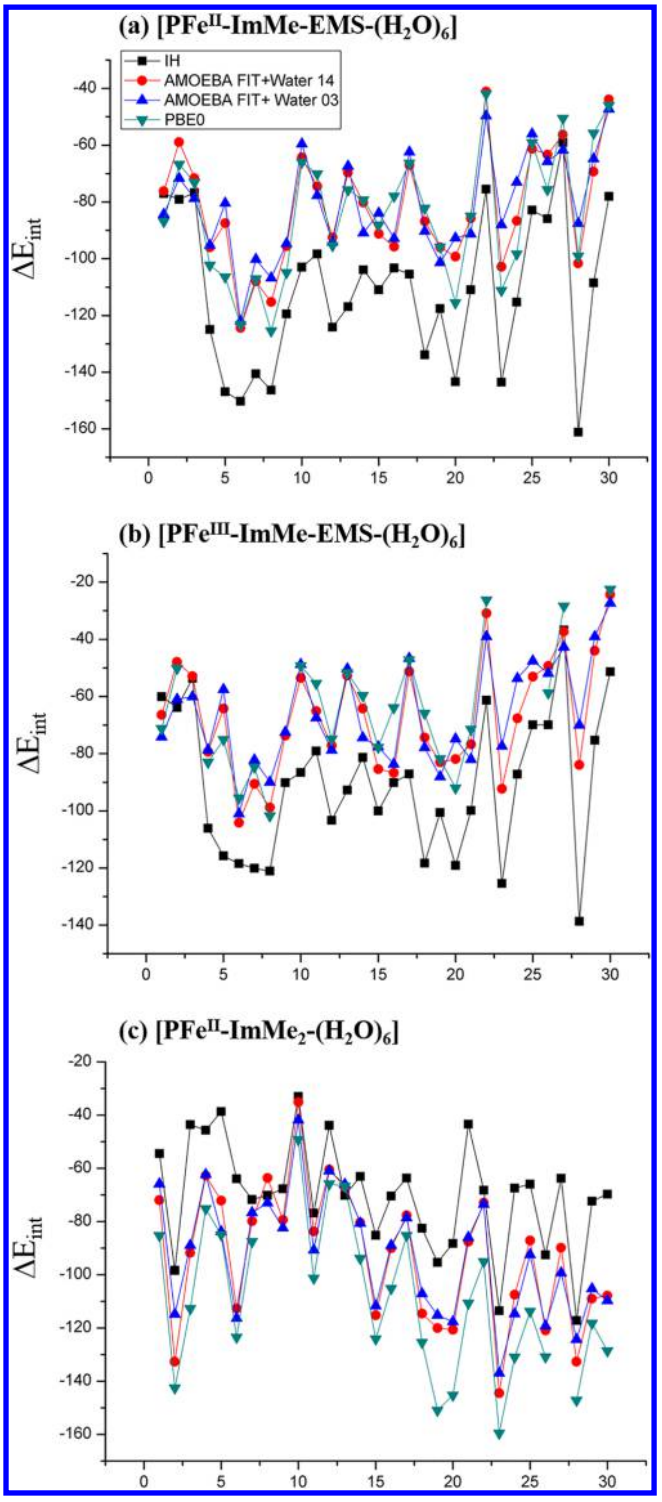

Figure 6. Interaction energies (kcal/mol) of the [PFe^{II}−ImMe−EMS−$(H_2O)_6$] (top), [PFe^{III}−ImMe−EMS−$(H_2O)_6$] (middle), and [PFe^{II}−$(ImMe)_2$−$(H_2O)_6$] (bottom) complexes with droplets of water molecules. For each complex, a collection of 30 geometries is considered.

a monopolar to a multipolar and polarizable description of the electrostatic potential created by the heme is beneficial for the accuracy of the force field. With the 2003 AMOEBA water model, the agreement is a little bit less satisfactory, with some points of the series departing more from the DFT results, but results are similar in nature and the set of investigated points limited. We emphasize that the same heme parameters are used in both series and that only the water model is changed. For the energies of present interest, the accuracy of the 2014 water model is superior. We note small differences between results obtained with either DMA or FIT sets of multipoles. Very similar conclusions can be drawn for the [PFe^{III}−ImMe−EMS−$(H_2O)_6$] complex with a better agreement of computed interaction energies with AMOEBA using the 2014 water model. Finally, for the [PFe^{II}−$(ImMe)_2$−$(H_2O)_6$] complex, we find that correlation between AMOEBA and DFT is much better than with nonpolarizable FF (R^2 = 0.94 vs 0.62). In summary, these calculations validate our parametrization approach for the heme complex. The computed interaction energies clearly indicate that the sets of multipoles are able to accurately reproduce the electrostatic potential created by the heme complex in both ferrous and ferric states.

III.D. Heme Coordination Patterns. Before moving in section IV to the simulation of hemeproteins with AMOEBA, we focus here on the inner-sphere coordination of the iron cation. We observed that in AMOEBA MD simulations of the [$PFe^{II/III}$−ImMe−EMS] complex in water, the (bi)squared pyramidal geometry around Fe is lost. This means that the sole presence of electrostatic multipoles on the heme atoms is not sufficient to define a proper coordination pattern for iron. This is somehow not surprising because the Fe−N or Fe−S bonds are more complex than resulting from a mere electrostatic interaction. We thus introduce supplementary terms in the potential energy between the iron atom and the two coordinating atoms in axial positions. To avoid the introduction of new atom classes in TINKER or TINKER-HP that would multiply the number of parameters, we have introduced the bonding and angle terms with the "Restrain" option of the program. A restraint term takes the form of a flat-welled harmonic potential. When we use the restrain option, we provide a force constant in kcal/Å^2 and two distances to define a distance range. If the distance between the two atoms under consideration is in this range, the energy from the restraint potential is zero. Outside the distance bounds, a standard harmonic term is used using the force constant and the interatomic distance. We have determined the parameters for the restraints by trial and error. We finally decided to restrain bonds between Fe and the coordinating atoms of the axial ligands (NE2 for histidine and SD for methionine) as well as the angles NE1−Fe−NE2 and NE1−Fe−SD where NE1 and NE2 are the porphyrin nitrogen atoms. The restraint parameters are given in Table S6.

Polarizable MD simulations have been performed with TINKER-HP (version 1.0).[49] The [PFe−ImMe−EMS] complex is immersed into a water box of edge length 24.875 Å. The Particle Mesh Ewald (PME) summation technique has been applied to treat electrostatic interactions, including polarization, with a real-space cutoff distance of 7.0 Å, a grid of 64 × 64 × 64, and fifth-order B-splines. A cutoff with a switching window at 10 Å has been applied to the van der Waals interactions. Induced dipoles have been iterated to convergence, until the Root-Mean-Square (RMS) change between interactions fell below 10^{-5} D per atom using the ASPC approach.[53] The trajectories have been propagated using a velocity form of Bernie Brook's "Better Beeman" integration algorithm with a 1.0 fs time step. The system temperature has been controlled with a Berendsen thermostat at 300 K.[86]

The average values and standard deviations of a few geometrical parameters of iron coordination are gathered in

DOI: 10.1021/acs.jctc.7b01128
J. Chem. Theory Comput. 2018, 14, 2705−2720

Table 3. Bond Lengths (in Å), Angles (in degree), and Doming Effect Dihedrals for the reduced and oxidized (Italic) eme Structure[a]

parameters	451C/351C[b]	mean X-ray[c]	DFT	PM7[d]	AMOEBA DMA	AMOEBA FIT
$Fe-N_{his}$	1.97	2.03 ± 0.15	1.97	1.97 (0.04)	2.07 (0.03)	2.06 (0.03)
	1.99		1.99		*2.05 (0.03)*	*2.03 (0.03)*
$Fe-S_{met}$	2.35	2.31 ± 0.18	2.28	2.33 (0.05)	2.39 (0.03)	2.39 (0.03)
	2.36		2.31		*2.38 (0.03)*	*2.38 (0.03)*
$Fe-N_{por}$	2.03	2.00 ± 0.05	2.00	1.95 (0.04)	2.10 (0.03)	2.10 (0.03)
	2.03		1.99		*2.10 (0.03)*	*2.10 (0.03)*
$N_{his}-Fe-N_{por}$	91.19	90 ± 2	89.89	89.88 (3.23)	90.10 (2.60)	90.10 (2.61)
	90.89		90.24		*89.72 (2.61)*	*89.88 (2.57)*
$S_{met}-Fe-N_{por}$	88.80	90 ± 2	90.10	90.12 (3.78)	89.99 (2.76)	89.87 (2.79)
	89.08		89.75		*90.39 (2.81)*	*90.12 (2.85)*
C2−Fe−C2	174.58	174 ± 3	174.71	177.81 (2.99)	177.65 (2.21)	176.26 (2.17)
	174.76		167.20		*176.09 (2.29)*	*176.17 (2.16)*
doming	0.04	0.04 ± 0.02[e]	0.01	0.051 (0.025)	0.04 (0.03)	0.04 (0.03)
	0.03		0.00		*0.04 (0.03)*	*0.04 (0.03)*

[a]For the PM7 and AMOEBA MD simulations, we provide average values and standard deviations (in parentheses). [b]Analysis of cyt C551 in both oxidized form (PDB 351) and reduced form (PDB 451C) were performed with VMD program. [c]Average variation observed in seven high resolution X-ray structures from ref FELIX (PDB: 5cyt, 1qn2, 3c2c, lio3, 1hro, 1c2r, 1cxc). [d]MD simulations showed that the coordination between Fe and the apical ligand is unphysical with the PM7 method in the ferric state. We thus do not report PM7 data for this redox state. Average variation observed in seven high resolution X-ray structures from 27. [e]Analysis using the seven structures used in ref 27.

Table 3. The upper part of the table refers to the bond distances and angles that were specifically restrained to a target value, while the lower part refers to other relevant parameters. Data for both redox states are provided. For comparison, we also provide similar values from an X-ray structure of cytochrome *c*551. The coordination around heme in this protein is representative and agrees well with the mean value of seven high resolution X-ray structures of other cytochromes containing the same heme group.[27] We also provide values extracted from the DFT optimized structure on which we fitted the sets of multipoles (Table 3) and average values obtained from MD simulations with PM7 (see previous subsection and SI).

The $Fe-N_{his}$, $Fe-N_{por}$, and $Fe-S_{met}$ average bond lengths obtained with AMOEBA DMA amount to 2.07, 2.10, and 2.39 Å, respectively, in the ferrous state. Similar values are obtained in the ferric state. These values are slightly larger than those obtained from PM7MD simulations or DFT geometry optimizations but within the experimental uncertainty of X-ray structures. The fluctuations of bond length are found to be on the order of 0.03 Å, in close agreement with PM7 simulations and on the order of the expected values for this type of chemical bonding. It could be possible to further increase the restraint force constants to further reduce the gap with DFT values, but we found that very strong force constants were needed to achieve this goal, probably because of repulsion between the axial ligand and the heme fragment originating from the van der Waals and permanent multipoles. It is still also possible that the distances are too long due to the lack of charge transfer between the metal and the porphyrin in the AMOEBA potential. Moreover, increasing the force constants would reduce too much the amplitude of the bond length fluctuations. We therefore decided to retain the set of restraints given in Table S6. The angles around the iron cation are also well reproduced by the AMOEBA simulations when comparing to the experimental and theoretical references. We find few differences for all these parameters when using either the AMOEBA DMA or AMOEBA FIT sets of multipoles. Regarding the C2−Fe−C2 angle (Figure 1) and the out-of-plane deformation of Fe (doming), we find slight displacement of the cation from the average plane of the porphyrin nitrogen atoms. We investigated also the energy profile corresponding to the rotation of the $C_{his}-N_{his}-Fe-N_{por}$ dihedral angle (Figure S2). The global minimum of the profile is located at 0° both at DFT and at AMOEBA levels of theory. The secondary minima are at the same positions with AMOEBA and PBE. The global potential well depth is more pronounced with AMOEBA than in DFT. However, we expect the dihedral distribution during a MD simulation to have similar behavior in AMOEBA and in DFT, centered around 0°, but slightly broader in DFT. Finally, we have inspected an extensive list of complementary geometrical parameters and found excellent agreement between AMOEBA and DFT or X-ray data (Tables S7).

IV. APPLICATION TO MD SIMULATIONS OF CYTOCHROME

In the last section of this article, we report simulations of cytochromes in the ferrous and ferric states with the newly developed AMOEBA FF parameters using the Tinker-HP program.[49] The FIT parameter sets are used. We consider cytochrome b_5 of *Rattus norvegicus* (PDB code: 1B5A[87]). The prosthetic group of cytochrome b_5 consists of a heme core with the two axial ligands being histidine residue side chains (His39 and His63). The initial structure has been extracted from NMR data and has been solvated in a cubic water box (edge length of 100 Å) using the CHARMM package.[88] The simulated system is comprised of 97 858 atoms. The protonation state of the residues has been evaluated with the PROPKa server. Aspartate and glutamate residues are deprotonated, while all histidine residues are protonated on δ positions. The system has been neutralized by adding 10 sodium cations. We have subsequently added nine (Na^+,Cl^-) ion pairs to reach a salt concentration of 0.15 M. The NMR structure has been preliminarily prepared using the nonpolarizable c31 CHARMM.[88] To this end, we have first carried out 10 000 steps of energy minimization with NAMD.[89] Equilibration has then been reached running successive 20 ps MD with a progressive increase of the temperature from 50 to 298 K by steps of 25 K. During the

DOI: 10.1021/acs.jctc.7b01128
J. Chem. Theory Comput. 2018, 14, 2705−2720

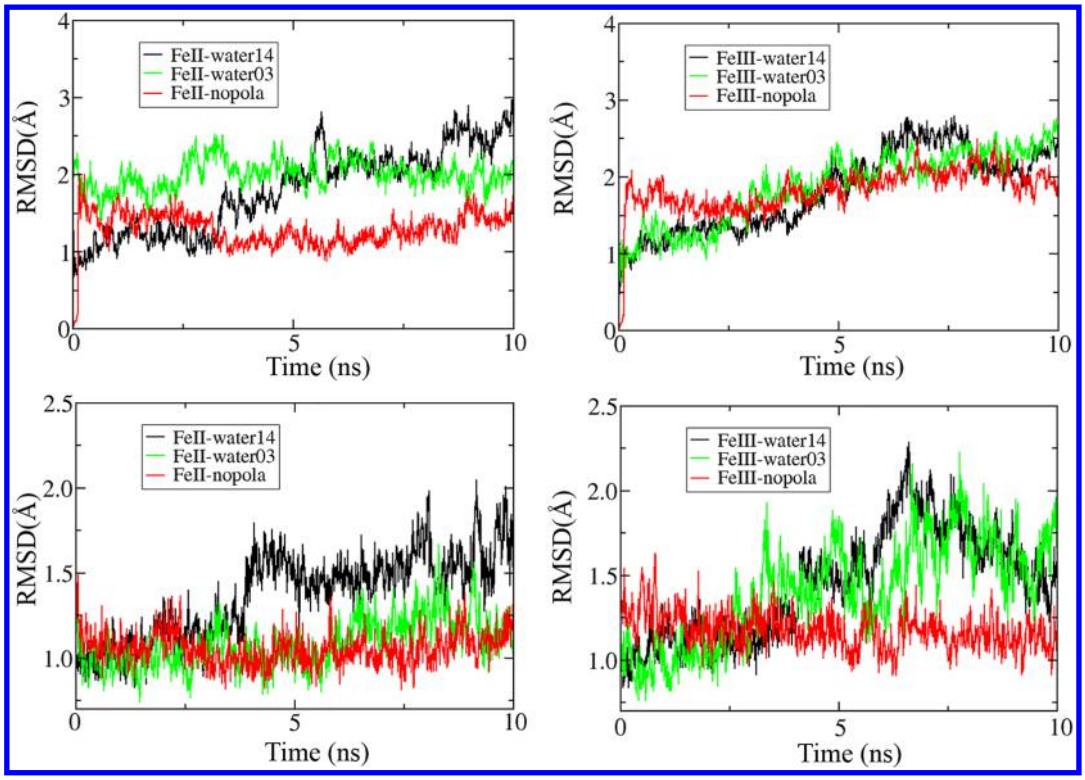

Figure 7. Upper panel, RMSD of protein backbone atoms. Lower panel, RMSD of protein backbone atoms belonging to alpha helices only. In all cases, the last seven residues that belong to a flexible loop were not included in the RMSD calculation.

Table 4. Bond Distance (Å) and Angle (degree) Values for Heme Structure[a]

			AMOEBA			
parameters	1B5A	DFT	Fe^{II} Water14	Fe^{III} Water14	Fe^{II} Water03	Fe^{III} Water03
$Fe-N_{his}$	2.00	1.97	2.07 (0.03)	2.05 (0.03)	2.07 (0.03)	2.05 (0.03)
$Fe-N_{por}$	2.00	2.01	2.10 (0.03)	2.11 (0.03)	2.10 (0.03)	2.11 (0.03)
$N_{his}-Fe-N_{por}$	90.03	90.00	90.00 (2.51)	89.99 (2.51)	90.00 (2.50)	89.86 (2.50)

[a]RMN structure. DFT optimized geometry and averaged over the trajectories of different MD simulations with the standard deviations (within parentheses).

heating, the protein heavy atoms have been kept fixed by adding harmonic restraints on their positions with force constants of 10 kcal/mol/Å^2. Subsequently, four successive MD simulations in the NPT ensemble have been conducted over 3 × 100 and 500 ps with restraint force constants of 10, 5, 1, and 0 kcal/mol/Å^2, respectively. A time step of 2 fs has been used. The final equilibrated structure is used as the starting geometry for AMOEBA polarizable simulations.

Simulations have been conducted in the two redox states and with either the water03 or water14 models. The same parameters as in the previous section are used, except that a RESPA integration algorithm allowing a 2.0 fs time step is used here. The temperature has been controlled by a Bussi thermostat.[90] The Particle Mesh Ewald (PME) summation technique has been applied to treat electrostatic interactions, including polarization, with a real-space cutoff distance of 7.0 Å, a grid of 64 × 64 × 64, and fifth-order B-splines. A cutoff with a switching window at 10 Å has been applied to the van der Waals interactions. Induced dipoles have been iterated to convergence, until the Root-Mean-Square (RMS) change between interactions fell below 10^{-5} D per atom and simulations used the ASPC approach. With the equilibrated structure obtained with the nonpolarizable FF, we have performed another equilibration procedure with AMOEBA parameters. For this, we have first fixed the hemeprotein, and have done energy minimization with a convergence value of 0.5 kcal mol^{-1} Å^{-1}. Equilibration has been obtained running successive 50 ps NVT MD with a progressive increase of the temperature from 50 to 300 K by steps of 50 K keeping hemeprotein fixed. Then, we have carried out another equilibration with the hemeprotein atom free to move. Finally, we have conducted an 80 ps NPT simulation at 300 K and 1 atm to obtain a stable density of the system (higher than 1 gr/cm^3). A 10 ns MD simulation in the NVT ensemble has been accumulated for analysis. Restraints on angles and bonds involving the iron cation have been set as explained in the previous section. For comparisons, we also carried out MD simulations with a nonpolarizable force field (CHARMM) using the NAMD program.[89]

The RMSDs of the protein backbone (focusing on residues 1 to 87) during MD simulation dynamics are shown in Figure 7. For each simulation, the RMSD value is below 3 Å. When focusing on amino acid residues pertaining to structured alpha helices, the RMSDs are, as expected, smaller. We have not noticed any unfolding of tertiary secondary structures during the simulations. Compared to simulations with nonpolarizable

DOI: 10.1021/acs.jctc.7b01128
J. Chem. Theory Comput. 2018, 14, 2705−2720

FF, the RMSDs show more slight fluctuations but remain on the same order. In regard to the heme coordination sphere, AMOEBA gives good agreement for bond lengths and angles with NMR and DFT data (Table 4, Table S8). The force constants adjusted to define the iron cation inner-sphere coordination are transferable to the heme embedded into the protein matrix. Overall, these data indicate stable dynamics with the here developed parameters in both ferrous and ferric forms. The atom RMSDs for amino acid residues localized within 10 Å are shown in Figure S3. They are examined by types of residues (polar, charged, apolar...). Again, we have not found any conformational changes of theses residues that would be suspicious. However, conformation fluctuations are often more pronounced for the AMOEBA force field, probably because of the more flexible form of the underlying potential energy function. Future works will have to consider much longer simulations to assess the stability of hemoproteins and to investigate whether the herein developed AMOEBA force field for heme leads to more accurate redox properties than standard force fields.

These MD simulations have been run using 1440 2.6-GHz processors connected via infinite band technology (IB 4x FDR). The total wall clock time was approximately 12 h/ns of simulation on the Occigen machine at CINES (Montpellier, France). We mention that recent algorithmic developments of Tinker-HP should further improve efficiency. MD simulation of hemeproteins with AMOEBA is now computationally feasible in reasonable times.

V. CONCLUSION

In this article, we have reported to our knowledge the first parameters of heme for the polarizable AMOEBA force field. They have been derived both for the ferrous and ferric forms. Extensive validation has been obtained from calculations of interaction energies with series of small molecules of biological interest and on large water aggregates comprising around 80 water molecules. We have found that the description of the electrostatic interaction with the heme is greatly improved with AMOEBA. This is especially noticeable regarding interaction energies with water aggregates for which the correlation with DFT results outperforms that of a nonpolarizable model. That said, we have also found the model for water to have strong influence on the accuracy of the computed interaction energies. The 2014 water model has been found to be in better agreement with the reported DFT reference calculations, although results obtained with the 2003 potential are similar in nature. We have finally reported MD simulation of a cytochrome using the AMOEBA force field.

The availability of parameters for heme combined with the advent of highly efficient implementation of AMOEBA in the TINKER-HP software opens the door to wide applications of MD simulations of hemeproteins with AMOEBA. The herein devised parameters are freely available in the SI or upon request to the authors.

■ ASSOCIATED CONTENT

Supporting Information

The Supporting Information is available free of charge on the ACS Publications website at DOI: 10.1021/acs.jctc.7b01128.

Computational protocol for PM7 simulations, tables of interaction energies for all the structures, restraint parameters for the inner-sphere coordination of the iron cation, AMOEBA multipoles for heme, autocorrelation function of AMOEBA interaction energies of heme with water droplets, energy profile associated to the rotation around the Nhis-Fe bond, RMSD of aminoacid residues during MD simulations of cytochrome (PDF)

■ AUTHOR INFORMATION

Corresponding Authors

*E-mail: carine.clavaguera@u-psud.fr.
*E-mail: aurelien.de-la-lande@u-psud.fr.

ORCID

Carine Clavaguera: 0000-0001-5531-2333
Jean-Philip Piquemal: 0000-0001-6615-9426
Aurélien de la Lande: 0000-0003-0745-4171

Notes

The authors declare no competing financial interest.

■ ACKNOWLEDGMENTS

Calculations were carried out at the French computer center CINES, France. We greatly acknowledge GENCI for providing us with generous computational resources (project number A0020706913).

■ REFERENCES

(1) Poulos, T. L. Heme Enzyme Structure and Function. *Chem. Rev.* **2014**, *114* (7), 3919−3962.
(2) Smith, L. J.; Kahraman, A.; Thornton, J. M. Heme proteins—Diversity in structural characteristics, function, and folding. *Proteins: Struct., Funct., Genet.* **2010**, *78* (10), 2349−2368.
(3) Loew, G. H.; Harris, D. L. Role of the Heme Active Site and Protein Environment in Structure, Spectra, and Function of the Cytochrome P450s. *Chem. Rev.* **2000**, *100* (2), 407−420.
(4) Van Doorslaer, S. Understanding heme proteins with hyperfine spectroscopy. *J. Magn. Reson.* **2017**, *280* (Supplement C), 79−88.
(5) Prytkova, T. R.; Kurnikov, I. V.; Beratan, D. N. Coupling Coherence Distinguishes Structure Sensitivity in Protein Electron Transfer. *Science* **2007**, *315* (5812), 622−625.
(6) Keinan, S.; Nocek, J. M.; Hoffman, B. M.; Beratan, D. N. Interfacial hydration, dynamics and electron transfer: multi-scale ET modeling of the transient [myoglobin, cytochrome b5] complex. *Phys. Chem. Chem. Phys.* **2012**, *14* (40), 13881−13889.
(7) Blumberger, J.; Klein, M. L. Reorganization Free Energies for Long-Range Electron Transfer in a Porphyrin-Binding Four-Helix Bundle Protein. *J. Am. Chem. Soc.* **2006**, *128* (42), 13854−13867.
(8) Tipmanee, V.; Oberhofer, H.; Park, M.; Kim, K. S.; Blumberger, J. Prediction of Reorganization Free Energies for Biological Electron Transfer: A Comparative Study of Ru-Modified Cytochromes and a 4-Helix Bundle Protein. *J. Am. Chem. Soc.* **2010**, *132* (47), 17032−17040.
(9) Breuer, M.; Zarzycki, P.; Blumberger, J.; Rosso, K. M. Thermodynamics of Electron Flow in the Bacterial Deca-heme Cytochrome MtrF. *J. Am. Chem. Soc.* **2012**, *134* (24), 9868−9871.
(10) Breuer, M.; Rosso, K. M.; Blumberger, J. Electron flow in multiheme bacterial cytochromes is a balancing act between heme electronic interaction and redox potentials. *Proc. Natl. Acad. Sci. U. S. A.* **2014**, *111* (2), 611−616.
(11) Derat, E.; Shaik, S.; Rovira, C.; Vidossich, P.; Alfonso-Prieto, M. The Effect of a Water Molecule on the Mechanism of Formation of Compound 0 in Horseradish Peroxidase. *J. Am. Chem. Soc.* **2007**, *129* (20), 6346−6347.
(12) Shaik, S.; Kumar, D.; de Visser, S. P.; Altun, A.; Thiel, W. Theoretical Perspective on the Structure and Mechanism of Cytochrome P450 Enzymes. *Chem. Rev.* **2005**, *105* (6), 2279−2328.

DOI: 10.1021/acs.jctc.7b01128
J. Chem. Theory Comput. 2018, 14, 2705−2720

(13) Mao, J.; Hauser, K.; Gunner, M. R. How Cytochromes with Different Folds Control Heme Redox Potentials. *Biochemistry* **2003**, *42* (33), 9829−9840.
(14) Song, Y.; Mao, J.; Gunner, M. R. Electrostatic Environment of Hemes in Proteins: pKas of Hydroxyl Ligands. *Biochemistry* **2006**, *45* (26), 7949−7958.
(15) Blumberger, J. Recent Advances in the Theory and Molecular Simulation of Biological Electron Transfer Reactions. *Chem. Rev.* **2015**, *115* (20), 11191−11238.
(16) Olsson, M. H. M.; Hong, G.; Warshel, A. Frozen Density Functional Free Energy Simulations of Redox Proteins: Computational Studies of the Reduction Potential of Plastocyanin and Rusticyanin. *J. Am. Chem. Soc.* **2003**, *125* (17), 5025−5039.
(17) Parson, W. W.; Chu, Z. T.; Warshel, A. Reorganization Energy of the Initial Electron-Transfer Step in Photosynthetic Bacterial Reaction Centers. *Biophys. J.* **1998**, *74* (1), 182−191.
(18) Blumberger, J. Free energies for biological electron transfer from QM/MM calculation: method, application and critical assessment. *Phys. Chem. Chem. Phys.* **2008**, *10* (37), 5651−5667.
(19) de la Lande, A.; Gillet, N.; Chen, S.; Salahub, D. R. Progress and challenges in simulating and understanding electron transfer in proteins. *Arch. Biochem. Biophys.* **2015**, *582*, 28−41.
(20) Warshel, A.; Kato, M.; Pisliakov, A. V. Polarizable Force Fields: History, Test Cases, and Prospects. *J. Chem. Theory Comput.* **2007**, *3* (6), 2034−2045.
(21) Warshel, A.; Parson, W. W. Computer Simulations of Electron-Transfer Reactions in Solution and in Photosynthetic Reaction Centers. *Annu. Rev. Phys. Chem.* **1991**, *42* (1), 279−309.
(22) Tipmanee, V.; Blumberger, J. Kinetics of the Terminal Electron Transfer Step in Cytochrome c Oxidase. *J. Phys. Chem. B* **2012**, *116* (6), 1876−1883.
(23) Oda, A.; Yamaotsu, N.; Hirono, S. New AMBER force field parameters of heme iron for cytochrome P450s determined by quantum chemical calculations of simplified models. *J. Comput. Chem.* **2005**, *26* (8), 818−826.
(24) Shahrokh, K.; Orendt, A.; Yost, G. S.; Cheatham, T. E. Quantum mechanically derived AMBER-compatible heme parameters for various states of the cytochrome P450 catalytic cycle. *J. Comput. Chem.* **2012**, *33* (2), 119−133.
(25) Kaszuba, K.; Postila, P. A.; Cramariuc, O.; Sarewicz, M.; Osyczka, A.; Vattulainen, I.; Róg, T. Parameterization of the prosthetic redox centers of the bacterial cytochrome bc 1 complex for atomistic molecular dynamics simulations. *Theor. Chem. Acc.* **2013**, *132* (6), 1370.
(26) Favia, A. D.; Cavalli, A.; Masetti, M.; Carotti, A.; Recanatini, M. Three-dimensional model of the human aromatase enzyme and density functional parameterization of the iron-containing protoporphyrin IX for a molecular dynamics study of heme-cysteinato cytochromes. *Proteins: Struct., Funct., Genet.* **2006**, *62* (4), 1074−1087.
(27) Autenrieth, F.; Tajkhorshid, E.; Baudry, J.; Luthey-Schulten, Z. Classical force field parameters for the heme prosthetic group of cytochrome c. *J. Comput. Chem.* **2004**, *25* (13), 1613−1622.
(28) Johansson, M. P.; Kaila, V. R. I.; Laakkonen, L. Charge parameterization of the metal centers in cytochrome c oxidase. *J. Comput. Chem.* **2008**, *29* (5), 753−767.
(29) Adam, S.; Knapp-Mohammady, M.; Yi, J.; Bondar, A.-N. Revised CHARMM force field parameters for iron-containing cofactors of photosystem II. *J. Comput. Chem.* **2018**, *39*, 7.
(30) Muegge, I.; Qi, P. X.; Wand, A. J.; Chu, Z. T.; Warshel, A. The Reorganization Energy of Cytochrome c Revisited. *J. Phys. Chem. B* **1997**, *101* (5), 825−836.
(31) Ponder, J. *TINKER - Software Tools for Molecular Design*, version 7.1.2.
(32) Ren, P.; Ponder, J. W. Polarizable Atomic Multipole Water Model for Molecular Mechanics Simulation. *J. Phys. Chem. B* **2003**, *107* (24), 5933−5947.
(33) Laury, M. L.; Wang, L.-P.; Pande, V. S.; Head-Gordon, T.; Ponder, J. W. Revised Parameters for the AMOEBA Polarizable Atomic Multipole Water Model. *J. Phys. Chem. B* **2015**, *119* (29), 9423−9437.
(34) Semrouni, D.; Isley, W. C.; Clavaguéra, C.; Dognon, J.-P.; Cramer, C. J.; Gagliardi, L. Ab Initio Extension of the AMOEBA Polarizable Force Field to Fe2+. *J. Chem. Theory Comput.* **2013**, *9* (7), 3062−3071.
(35) Grossfield, A.; Ren, P.; Ponder, J. W. Ion Solvation Thermodynamics from Simulation with a Polarizable Force Field. *J. Am. Chem. Soc.* **2003**, *125* (50), 15671−15682.
(36) Clavaguéra, C.; Calvo, F.; Dognon, J.-P. Theoretical study of the hydrated Gd3+ ion: Structure, dynamics, and charge transfer. *J. Chem. Phys.* **2006**, *124* (7), 074505.
(37) Piquemal, J.-P.; Perera, L.; Cisneros, G. A.; Ren, P.; Pedersen, L. G.; Darden, T. A. Towards accurate solvation dynamics of divalent cations in water using the polarizable amoeba force field: From energetics to structure. *J. Chem. Phys.* **2006**, *125* (5), 054511.
(38) Wu, J. C.; Piquemal, J.-P.; Chaudret, R.; Reinhardt, P.; Ren, P. Polarizable Molecular Dynamics Simulation of Zn(II) in Water Using the AMOEBA Force Field. *J. Chem. Theory Comput.* **2010**, *6* (7), 2059−2070.
(39) Ponder, J. W.; Wu, C.; Ren, P.; Pande, V. S.; Chodera, J. D.; Schnieders, M. J.; Haque, I.; Mobley, D. L.; Lambrecht, D. S.; DiStasio, R. A.; Head-Gordon, M.; Clark, G. N. I.; Johnson, M. E.; Head-Gordon, T. Current Status of the AMOEBA Polarizable Force Field. *J. Phys. Chem. B* **2010**, *114* (8), 2549−2564.
(40) Satpati, P.; Clavaguéra, C.; Ohanessian, G.; Simonson, T. Free Energy Simulations of a GTPase: GTP and GDP Binding to Archaeal Initiation Factor 2. *J. Phys. Chem. B* **2011**, *115* (20), 6749−6763.
(41) Zhang, J.; Yang, W.; Piquemal, J.-P.; Ren, P. Modeling Structural Coordination and Ligand Binding in Zinc Proteins with a Polarizable Potential. *J. Chem. Theory Comput.* **2012**, *8* (4), 1314−1324.
(42) Ren, P.; Wu, C.; Ponder, J. W. Polarizable Atomic Multipole-Based Molecular Mechanics for Organic Molecules. *J. Chem. Theory Comput.* **2011**, *7* (10), 3143−3161.
(43) Shi, Y.; Xia, Z.; Zhang, J.; Best, R.; Wu, C.; Ponder, J. W.; Ren, P. Polarizable Atomic Multipole-Based AMOEBA Force Field for Proteins. *J. Chem. Theory Comput.* **2013**, *9* (9), 4046−4063.
(44) Lamoureux, G.; Roux, B. t. Modeling induced polarization with classical Drude oscillators: Theory and molecular dynamics simulation algorithm. *J. Chem. Phys.* **2003**, *119* (6), 3025−3039.
(45) Blumberger, J.; Lamoureux, G. Reorganization free energies and quantum corrections for a model electron self-exchange reaction: comparison of polarizable and non-polarizable solvent models. *Mol. Phys.* **2008**, *106* (12−13), 1597−1611.
(46) Wang, Q.; Rackers, J. A.; He, C.; Qi, R.; Narth, C.; Lagardere, L.; Gresh, N.; Ponder, J. W.; Piquemal, J.-P.; Ren, P. General Model for Treating Short-Range Electrostatic Penetration in a Molecular Mechanics Force Field. *J. Chem. Theory Comput.* **2015**, *11* (6), 2609−2618.
(47) Narth, C.; Lagardère, L.; Polack, É.; Gresh, N.; Wang, Q.; Bell, D. R.; Rackers, J. A.; Ponder, J. W.; Ren, P. Y.; Piquemal, J.-P. Scalable improvement of SPME multipolar electrostatics in anisotropic polarizable molecular mechanics using a general short-range penetration correction up to quadrupoles. *J. Comput. Chem.* **2016**, *37* (5), 494−506.
(48) Rackers, J. A.; Wang, Q.; Liu, C.; Piquemal, J.-P.; Ren, P.; Ponder, J. W. An optimized charge penetration model for use with the AMOEBA force field. *Phys. Chem. Chem. Phys.* **2017**, *19* (1), 276−291.
(49) Lagardère, L.; Jolly, L.-H.; Lipparini, F.; Aviat, F.; Stamm, B.; Jing, Z. F.; Harger, M.; Torabifard, H.; Cisneros, G. A.; Schnieders, M. J.; Gresh, N.; Maday, Y.; Ren, P. Y.; Ponder, J. W.; Piquemal, J.-P. Tinker-HP: a massively parallel molecular dynamics package for multiscale simulations of large complex systems with advanced point dipole polarizable force fields. *Chem. Sci.* **2018**, *9* (4), 956−972.
(50) Lipparini, F.; Lagardère, L.; Stamm, B.; Cancès, E.; Schnieders, M.; Ren, P.; Maday, Y.; Piquemal, J.-P. Scalable Evaluation of Polarization Energy and Associated Forces in Polarizable Molecular Dynamics: I. Toward Massively Parallel Direct Space Computations. *J. Chem. Theory Comput.* **2014**, *10* (4), 1638−1651.

DOI: 10.1021/acs.jctc.7b01128
J. Chem. Theory Comput. 2018, 14, 2705−2720

(51) Lagardère, L.; Lipparini, F.; Polack, É.; Stamm, B.; Cancès, É.; Schnieders, M.; Ren, P.; Maday, Y.; Piquemal, J.-P. Scalable Evaluation of Polarization Energy and Associated Forces in Polarizable Molecular Dynamics: II. Toward Massively Parallel Computations Using Smooth Particle Mesh Ewald. *J. Chem. Theory Comput.* **2015**, *11* (6), 2589−2599.
(52) Allinger, N. L.; Yuh, Y. H.; Lii, J. H. Molecular mechanics. The MM3 force field for hydrocarbons. 1. *J. Am. Chem. Soc.* **1989**, *111* (23), 8551−8566.
(53) Kolafa, J. Time-reversible always stable predictor−corrector method for molecular dynamics of polarizable molecules. *J. Comput. Chem.* **2004**, *25* (3), 335−342.
(54) Thole, B. T. Molecular polarizabilities calculated with a modified dipole interaction. *Chem. Phys.* **1981**, *59* (3), 341−350.
(55) Wu, J. C.; Chattree, G.; Ren, P. Automation of AMOEBA polarizable force field parameterization for small molecules. *Theor. Chem. Acc.* **2012**, *131* (3), 1138.
(56) Bultinck, P.; Van Alsenoy, C.; Ayers, P. W.; Carbó-Dorca, R. Critical analysis and extension of the Hirshfeld atoms in molecules. *J. Chem. Phys.* **2007**, *126* (14), 144111.
(57) Hoe, W.-M.; Cohen, A. J.; Handy, N. C. Assessment of a new local exchange functional OPTX. *Chem. Phys. Lett.* **2001**, *341* (3), 319−328.
(58) Perdew, J. P.; Burke, K.; Ernzerhof, M. Generalized Gradient Approximation Made Simple. *Phys. Rev. Lett.* **1996**, *77* (18), 3865−3868.
(59) Calaminici, P.; Janetzko, F.; Köster, A. M.; Mejia-Olvera, R.; Zuniga-Gutierrez, B. Density functional theory optimized basis sets for gradient corrected functionals: 3d transition metal systems. *J. Chem. Phys.* **2007**, *126* (4), 044108.
(60) Koster, A. M.; Calaminici, P.; Casida, M. E.; Dominguez, V. D.; Flores-Moreno, R.; Geudtner, G.; Goursot, A.; Heine, T.; Ipatov, A.; Janetzko, F.; del Campo, J. M.; Reveles, J. U.; Vela, A.; Zuniga-Gutierrez, B.; Salahub, D. R. *deMon2k*, version 2; The deMon Developers: Mexico City, 2011.
(61) Abdurahman, A.; Renger, T. Density Functional Studies of Iron-Porphyrin Cation with Small Ligands X (X: O, CO, NO, O2, N2, H2O, N2O, CO2). *J. Phys. Chem. A* **2009**, *113* (32), 9202−9206.
(62) Conradie, J.; Ghosh, A. Electronic Structure of Trigonal-Planar Transition-Metal−Imido Complexes: Spin-State Energetics, Spin-Density Profiles, and the Remarkable Performance of the OLYP Functional. *J. Chem. Theory Comput.* **2007**, *3* (3), 689−702.
(63) Köster, A. M.; Reveles, J. U.; del Campo, J. M. Calculation of exchange-correlation potentials with auxiliary function densities. *J. Chem. Phys.* **2004**, *121* (8), 3417−3424.
(64) Frisch, M. J.; Trucks, G. W.; Schlegel, H. B.; Scuseria, G. E.; Robb, M. A.; Cheeseman, J. R.; Scalmani, G.; Barone, V.; Mennucci, B.; Petersson, G. A.; Nakatsuji, H.; Caricato, M.; Li, X.; Hratchian, H. P.; Izmaylov, A. F.; Bloino, J.; Zheng, G.; Sonnenberg, J. L.; Hada, M.; Ehara, M.; Toyota, K.; Fukuda, R.; Hasegawa, J.; Ishida, M.; Nakajima, T.; Honda, Y.; Kitao, O.; Nakai, H.; Vreven, T.; Montgomery, J. A., Jr.; Peralta, J. E.; Ogliaro, F. O.; Bearpark, M. J.; Heyd, J.; Brothers, E. N.; Kudin, K. N.; Staroverov, V. N.; Kobayashi, R.; Normand, J.; Raghavachari, K.; Rendell, A. P.; Burant, J. C.; Ayengar, S. S.; Tomasi, J.; Cossi, M.; Rega, N.; Millam, N. J.; Klene, M.; Knox, J. E.; Cross, J. B.; Bakken, V.; Adamo, C.; Jaramillo, J.; Gomperts, R.; Stratmann, R. E.; Yazyev, O.; Austin, A. J.; Cammi, R.; Pomelli, C.; Ochterski, J. W.; Martin, R. L.; Morokuma, K.; Zakrzewski, V. G.; Voth, G. A.; Salvador, P.; Dannenberg, J. J.; Dapprich, S.; Daniels, A. D.; Farkas, O.; Foresman, J. B.; Ortiz, J. V.; Cioslowski, J.; Fox, D. J. *Gaussian 09*; Gaussian, Inc.: Wallingford, CT, 2009.
(65) Stone, A. J. Distributed Multipole Analysis: Stability for Large Basis Sets. *J. Chem. Theory Comput.* **2005**, *1* (6), 1128−1132.
(66) Stone, A. J.; Dullweber, A.; Engkvist, O.; Fraschini, E.; Hodges, M. P.; Meredith, A. W.; Nutt, D. R.; Popelier, P. L. A.; Wales, D. J. *Orient: a program for studying interactions between molecules*, version 4.5; University of Cambridge, 2002.
(67) Stone, A. J. Distributed multipole analysis, or how to describe a molecular charge distribution. *Chem. Phys. Lett.* **1981**, *83* (2), 233−239.
(68) Stone, A. J.; Alderton, M. Distributed multipole analysis. *Mol. Phys.* **1985**, *56* (5), 1047−1064.
(69) Semrouni, D.; Sharma, A.; Dognon, J.-P.; Ohanessian, G.; Clavaguéra, C. Finite Temperature Infrared Spectra from Polarizable Molecular Dynamics Simulations. *J. Chem. Theory Comput.* **2014**, *10* (8), 3190−3199.
(70) Ermler, U.; Siddiqui, R. A.; Cramm, R.; Friedrich, B. Crystal structure of the flavohemoglobin from Alcaligenes eutrophus at 1.75 A resolution. *EMBO J.* **1995**, *14* (24), 6067−6077.
(71) El Hammi, E.; Houee-Levin, C.; Rezac, J.; Levy, B.; Demachy, I.; Baciou, L.; de la Lande, A. New insights into the mechanism of electron transfer within flavohemoglobins: tunnelling pathways, packing density, thermodynamic and kinetic analyses. *Phys. Chem. Chem. Phys.* **2012**, *14* (40), 13872−13880.
(72) Iwata, S.; Ostermeier, C.; Ludwig, B.; Michel, H. Structure at 2.8 Å resolution of cytochrome c oxidase from Paracoccus denitrificans. *Nature* **1995**, *376*, 660.
(73) Becke, A. D. A new mixing of Hartree−Fock and local density-functional theories. *J. Chem. Phys.* **1993**, *98* (2), 1372−1377.
(74) Furche, F.; Ahlrichs, R.; Hättig, C.; Klopper, W.; Sierka, M.; Weigend, F. Turbomole. *Wiley Interdisciplinary Reviews: Computational Molecular Science* **2014**, *4* (2), 91−100.
(75) Köster, A. M.; Flores-Moreno, R.; Reveles, J. U. Efficient and reliable numerical integration of exchange-correlation energies and potentials. *J. Chem. Phys.* **2004**, *121* (2), 681−690.
(76) Mejía-Rodríguez, D.; Köster, A. M. Robust and efficient variational fitting of Fock exchange. *J. Chem. Phys.* **2014**, *141* (12), 124114.
(77) de la Lande, A.; Clavaguéra, C.; Köster, A. On the accuracy of population analyses based on fitted densities. *J. Mol. Model.* **2017**, *23* (4), 99.
(78) Humphrey, W.; Dalke, A.; Schulten, K. VMD: Visual molecular dynamics. *J. Mol. Graphics* **1996**, *14* (1), 33−38.
(79) Řezáč, J. Cuby: An integrative framework for computational chemistry. *J. Comput. Chem.* **2016**, *37* (13), 1230−1237.
(80) Adamo, C.; Barone, V. Toward reliable density functional methods without adjustable parameters: The PBE0 model. *J. Chem. Phys.* **1999**, *110* (13), 6158−6170.
(81) Yuan, D.; Li, Y.; Ni, Z.; Pulay, P.; Li, W.; Li, S. Benchmark Relative Energies for Large Water Clusters with the Generalized Energy-Based Fragmentation Method. *J. Chem. Theory Comput.* **2017**, *13* (6), 2696−2704.
(82) Chai, J.-D.; Head-Gordon, M. Systematic optimization of long-range corrected hybrid density functionals. *J. Chem. Phys.* **2008**, *128* (8), 084106.
(83) Vydrov, O. A.; Scuseria, G. E. Assessment of a long-range corrected hybrid functional. *J. Chem. Phys.* **2006**, *125* (23), 234109.
(84) Grimme, S.; Antony, J.; Ehrlich, S.; Krieg, H. A consistent and accurate ab initio parametrization of density functional dispersion correction (DFT-D) for the 94 elements H-Pu. *J. Chem. Phys.* **2010**, *132* (15), 154104.
(85) Zhao, Y.; Schultz, N. E.; Truhlar, D. G. Design of Density Functionals by Combining the Method of Constraint Satisfaction with Parametrization for Thermochemistry, Thermochemical Kinetics, and Noncovalent Interactions. *J. Chem. Theory Comput.* **2006**, *2* (2), 364−382.
(86) Berendsen, H. J. C.; Postma, J. P. M.; van Gunsteren, W. F.; DiNola, A.; Haak, J. R. Molecular dynamics with coupling to an external bath. *J. Chem. Phys.* **1984**, *81* (8), 3684−3690.
(87) Dangi, B.; Sarma, S.; Yan, C.; Banville, D. L.; Guiles, R. D. The Origin of Differences in the Physical Properties of the Equilibrium Forms of Cytochrome b5 Revealed through High-Resolution NMR Structures and Backbone Dynamic Analyses. *Biochemistry* **1998**, *37* (23), 8289−8302.
(88) Brooks, B. R.; Brooks, C. L.; Mackerell, A. D.; Nilsson, L.; Petrella, R. J.; Roux, B.; Won, Y.; Archontis, G.; Bartels, C.; Boresch,

DOI: 10.1021/acs.jctc.7b01128
J. Chem. Theory Comput. 2018, 14, 2705−2720

S.; Caflisch, A.; Caves, L.; Cui, Q.; Dinner, A. R.; Feig, M.; Fischer, S.; Gao, J.; Hodoscek, M.; Im, W.; Kuczera, K.; Lazaridis, T.; Ma, J.; Ovchinnikov, V.; Paci, E.; Pastor, R. W.; Post, C. B.; Pu, J. Z.; Schaefer, M.; Tidor, B.; Venable, R. M.; Woodcock, H. L.; Wu, X.; Yang, W.; York, D. M.; Karplus, M. CHARMM: The biomolecular simulation program. *J. Comput. Chem.* **2009**, *30* (10), 1545−1614.

(89) Phillips, J. C.; Braun, R.; Wang, W.; Gumbart, J.; Tajkhorshid, E.; Villa, E.; Chipot, C.; Skeel, R. D.; Kalé, L.; Schulten, K. Scalable molecular dynamics with NAMD. *J. Comput. Chem.* **2005**, *26* (16), 1781−1802.

(90) Bussi, G.; Parrinello, M. Stochastic thermostats: comparison of local and global schemes. *Comput. Phys. Commun.* **2008**, *179* (1), 26−29.

DOI: 10.1021/acs.jctc.7b01128
J. Chem. Theory Comput. 2018, 14, 2705−2720